eNeuro

Research Article: New Research | Disorders of the Nervous System

3D Visualization of Individual Regenerating Retinal Ganglion Cell Axons Reveals Surprisingly Complex Growth Paths

3D Reconstruction of Individual Regenerating Axons

Eric R. Bray[1], Markus Noga[1], Kinjal Thakor[1], Yun-Fang Wang[1], Vance P. Lemmon[1], Kevin K. Park[1] and Pantelis Tsoulfas[1]

[1]*Department of Neurological Surgery, Miami Project to Cure Paralysis, University of Miami Miller School of Medicine, Miami, FL 33136, USA*

DOI: 10.1523/ENEURO.0093-17.2017

Received: 20 March 2017

Revised: 28 July 2017

Accepted: 1 August 2017

Published: 21 August 2017

Author contributions: ERB, VPL, KKP and PT designed the research; ERB, YFW, and PT preformed the research; ERB, MN, KT, and PT analyzed the data; ERB, VPL, KKP and PT wrote the paper with input from other authors.

Funding: HHS | NIH | National Eye Institute (NEI): 100000053; 1R01EY022961. HHS | NIH | National Eye Institute (NEI): 100000053; 1R21EY026668. HHS | NIH | National Eye Institute (NEI): 100000053; 1U01EY027257. HHS | NIH | National Eye Institute (NEI): 100000053; 1F30EY025527. E. Matilda Ziegler Foundation for the Blind (EMZ Foundation): 100010310. Glaucoma Research Foundation (GRF): 100001641. Pew Charitable Trusts: 100000875. Buoniconti Fund to Cure Paralysis: 100001013.

Conflict of Interest: Authors report no conflict of interest.

Corresponding authors: Pantelis Tsoulfas, ptsoulfa@med.miami.edu or Kevin K. Park, kpark@med.miami.edu

Cite as: eNeuro 2017; 10.1523/ENEURO.0093-17.2017

3D Visualization of Individual Regenerating Retinal Ganglion Cell Axons Reveals Surprisingly Complex Growth Paths

Abbreviated title: 3D Reconstruction of Individual Regenerating Axons

Eric R. Bray[1], Markus Noga[1], Kinjal Thakor[1], Yun-Fang Wang[1], Vance P. Lemmon[1], Kevin K. Park[1,*], Pantelis Tsoulfas[1,*]

[1]Department of Neurological Surgery, Miami Project to Cure Paralysis
University of Miami Miller School of Medicine, Miami, FL 33136, USA
*** Corresponding authors:** ptsoulfa@med.miami.edu, kpark@med.miami.edu

Author contributions

ERB, VPL, KKP and PT designed the research; ERB, YFW, and PT preformed the research; ERB, MN, KT, and PT analyzed the data; ERB, VPL, KKP and PT wrote the paper with input from other authors.

Number of Figures: 7
Number of Tables: 1
Number of words for Abstract: 218
Number of words for Significance Statement: 120
Number of words for Introduction: 506
Number of words for Discussion: 1929

Acknowledgments:
This work was supported by grants from NEI 1R01EY022961-01 (KKP), NEI 1R21EY026668-01 (KKP), NEI 1U01EY027257-01 (KKP and VPL), NEI 1F30EY025527-01 (ERB), Walter G Ross Foundation (VPL), Ziegler Foundation (KKP), Glaucoma Research Foundation (KKP) and Pew Charitable Trust (KKP), The Miami Project to Cure Paralysis, and the Buoniconti Fund (KKP, VPL, and PT). The authors thank Pingping Jia at the University of Miami Viral Vector Core, and Melissa Carballosa-Gautam at the Miami Project
Conflicts of Interest: Authors report no conflict of interest

3D Visualization of Individual Regenerating Retinal Ganglion Cell Axons Reveals Surprisingly Complex Growth Paths

Abstract

Retinal ganglion cells (RGCs), the sole output cells of the retina, are a heterogeneous population of neurons that project axons to visual targets in the brain. Like most central nervous system (CNS) neurons, RGCs are considered incapable of mounting long distance axon regeneration. Using immunolabeling-enabled three-dimensional imaging of solvent-cleared organs (iDISCO) in transgenic mice, we tracked the entire paths of individual RGC axons and show that adult RGCs are highly capable of spontaneous long-distance regeneration, even without any treatment. Our results show that the Thy1-H-YFP mouse sparsely labels RGCs, consisting predominantly of regeneration-competent alpha type-RGCs (αRGCs). Following optic nerve crush, many of the YFP-labeled RGC axons extend considerable distances proximal to the injury site with only a few penetrating through the lesion. This tortuous axon growth proximal to the lesion site is even more striking with intravitreal ciliary neurotrophic factor (CNTF) treatment. We further demonstrate that despite traveling more than 5 mm (i.e. a distance equal to the length of mouse optic nerve), many of these circuitous axons are confined to the injury area and fail to reach the brain. Our results re-evaluate the view that RGCs are naturally incapable of re-extending long axons, and shift the focus from promoting axon elongation, to understanding factors that prevent direct growth of axons through the lesion and the injured nerve.

Significance Statement

Retinal ganglion cells (RGCs) are viewed as being incapable of mounting lengthy axon regeneration. Using whole tissue immunolabeling, we establish a technique to visualize and trace the entire paths of small populations of genetically labeled RGC axons as they regenerate. Following optic nerve injury, few axons grow beyond the lesion, but we find these axons branch and form loops proximal to the lesion. A regeneration inducing treatment further exacerbates branching and tortuous growth, while only modestly increasing the number of RGC axons that successfully grow beyond the lesion. Our study demonstrates extensive and circuitous RGC axon elongation both in pre- and post-lesion regions, highlighting the need to better understand the factors that inhibit direct axon growth in the optic nerve.

Introduction

Lack of axon regeneration is a major obstacle preventing functional recovery after axon injury. Like other neurons in the central nervous system (CNS), it is thought that retinal ganglion cells (RGCs) have a limited ability to regenerate spontaneously. Nonetheless, growth factors or modification of genes promote RGC axonal regeneration, to some extent. For example, supplying RGCs with cytokines, or genetic modification of *Pten, Pcaf, Stat3, Socs3, c-Myc, dcxl* or *Klf4* allows some RGC axons to regenerate with few axons reaching the brain targets (Park et al., 2008; Moore et al., 2009; Smith et al., 2009; Puttagunta et al., 2014; Belin et al., 2015; Nawabi et al., 2015; Leibinger et al., 2016; Mehta et al., 2016).

Multiple reports have demonstrated that some regenerating RGC axons travel circuitously within the optic nerve after intraorbital crush injury (Luo et al., 2013; Pernet et al., 2013). However, these studies have used anterograde tracers that label all RGC axons, making it difficult to identify individual fibers and visualize how axons of different RGC types behave as they regenerate. Here we sought to combine sparse neuronal labeling with the immunolabeling-enabled three-dimensional imaging of solvent-cleared organs (iDISCO) technique (Renier et al., 2016) and trace the entire path of individual axons as they regenerate.

RGCs are a heterogeneous population of neurons. They are divided into several subclasses based on their morphological, physiological, and molecular properties. Previous studies have shown that different RGC types differ in their ability to regenerate axons. For instance, studies in cats have shown that αRGCs regenerate axons better than other RGC types (Watanabe and Fukuda, 2002). Similarly, in mice it was demonstrated that αRGCs have greater propensity to regenerate axons after crush injury (Duan et al., 2015). RGCs in the Thy1-H-YFP mouse line have a "Golgi-like" labeling, allowing for the characterization of their dendrites and axons. Importantly,

this line labels few RGCs, most of which are immune-positive for SMI-32, a marker of αRGCs (Feng et al., 2000; Lin et al., 2004; Coombs et al., 2006).

In this study, we first validate that the Thy1-H-YFP mouse sparsely labels αRGCs. We used a combination of confocal imaging and iDISCO to analyze the dendrites and axons of the labeled neurons. We find that, after optic nerve crush; i) αRGC dendrites decrease in complexity, and the dendritic arbors are even less complex in animals treated with an axon growth promoting-stimulator (i.e. CNTF), ii) innately, axons remodel and regrow extensively proximal to the crush site, iii) following CNTF, axon elongation is extremely circuitous, and these axons never reach the brain, despite growing distances that would allow them to reach the brain, had they grown straight. Overall, our results show that RGCs can re-extend axons very well, even in the absence of a growth stimulator, but their inability to traverse the lesion area along with meandering axon growth limit "meaningful" regeneration, dramatically reducing the number of RGCs successfully regenerating axons into the brain. Our results shift the focus from promoting axon elongation, to understanding factors that prevent direct growth of CNS axons through the injured nerve.

Materials and Methods

Animals: All experimental procedures were performed in compliance with protocols approved by the Institutional Animal Care and Use Committee (IACUC) at the University of Miami. The Thy1-H-YFP mouse strain was used for all experiments (Jackson Laboratory stock number: 003782). All animals were housed in a viral antigen free facility and kept under standard 12-hour light-dark conditions. For all surgical procedures mice where anaesthetized with ketamine and xylazine. For analgesia, buprenorphine (0.05 mg/kg) was administered post-operatively. The exact number of animals used for each group is in the main text and figure legends.

Intravitreal Injection: Female and male mice 6 to 8 weeks old underwent unilateral intravitreal adeno-associated virus serotype 2 (AAV) injection. AAVs carried expression constructs for ciliary neurotrophic factor (CNTF) (AAV-CNTF)(Yungher et al., 2015) or placental alkaline phosphatase (PLAP) as a control transgene (AAV-PLAP). AAVs were made by the University of Miami's Viral Vector Core. Typical titers were 5 X 10^{12} GC/ml. A fine glass micropipette was inserted into the posterior chamber taking care to avoid damaging the lens. Using a Hamilton syringe (Hamilton 80900) 2 µl of virus was slowly injected. Cholera toxin beta conjugated to Alexa-594 (CTB) (ThermoFisher C34777, 2µg/µl in PBS) was injected as described above. CTB was injected 1 hour post crush in the 3dpc group.

Optic Nerve Crush: Animals received unilateral optic nerve crush. Time points post crush included in this study: 3 days post crush (3dpc), 3 weeks post crush (3wpc), and 6 weeks post crush (6wpc). AAV was injected 7 days before crush in the 3dpc group, or 3 days before crush in the 3wpc and 6wpc groups. For the optic nerve crush procedure, the optic nerve was exposed intra-orbitally by blunt dissection. The optic nerve was crushed with forceps (#5 Dumont, Fine Science Tools) for 10 seconds approximately 1 mm distal to the emergence from the globe.

Immunohistochemistry: Mice were euthanized by transcardial perfusion with ice cold PBS and 4% paraformaldehyde. The optic nerve was cut proximal to the optic chiasm. The globe with attached optic nerve was post-fixed in 4% paraformaldehyde overnight at 4°C. For retinal whole mount staining, the retina was carefully dissected out of the globe and derestricting cuts were placed in each quadrant. Tissue was washed with PBS and blocked in 5% normal donkey serum (Sigma D9663) in PBS + 0.3% Triton-X100 (PBST). Tissue was then incubated in blocking buffer containing primary antibodies, overnight at 4°C. Primary antibodies: Goat-anti-osteopontin (OSPN) 1:500 (R&D Systems, AF808), Rabbit-anti-melanopsin (OPN4) (UF006)

1:2,500 (Advanced Targeting Systems, AB-N38), Goat-anti-GFP 1:1,000 (Abcam, ab6673), Rabbit-anti-GFP 1:1,000 (Millipore, ab3080), Rabbit-anti-cocaine- and amphetamine-regulated transcript (CART) (55-102) 1:1,000 (Phoenix Pharmaceuticals, H-003-62). Following incubation with primary antibody, tissue was washed extensively in PBST. Tissue was then incubated in blocking buffer containing secondary antibodies 1:500, overnight at 4°C. Secondary antibodies: Donkey-anti-Rabbit Alexa-488 (ThermoFisher, A-21206), Donkey-anti-Rabbit Alexa-647 (ThermoFisher, A-31573), Donkey-anti-Goat Alexa-488 (ThermoFisher, A-11055), Donkey-anti-Goat Alexa-647 (ThermoFisher, A-21447). Following secondary incubation retinas were extensive washed with PBST, mounted with Slowfade (ThermoFisher, S36973) and coverslipped. Imaging was performed on an Olympus FV1000 confocal microscope, objectives: UPlanSApo 10X 0.40 N.A. and UPlanFLN 40X 1.3 N.A., and Olympus FV10-ASW Ver 0.200C software. Images were analyzed using Imaris software (Bitplane). Figures were composed using Photoshop CS6 (Adobe) and Illustrator CS5 (Adobe).

RGC quantification: The number of YFP^+ RGCs per retina was quantified from low magnification z-stack images that tiled the entire retina using an Olympus Fluoview 1000 confocal microscope. RGCs were defined by: soma location in the ganglion cell layer or inner nuclear layer (displaced RGC), and the presence of an axon. To determine the subtype of YFP^+ RGCs, every YFP^+ RGC in a retina was assessed for immunoreactivity with a RGC subtype marker: OSPN, Opn4, or CART (*See results for n number of retinas assessed for each marker)*. Survival of YFP^+ RGCs was determined as the number of YFP^+ RGCs remaining or the percentage of YFP^+ RGCs remaining compared to the uninjured contralateral retina. To analyze RGC dendrites high magnification z-stack images were taken of individual RGCs from the retinal nerve fiber layer to the inner nuclear layer. Images were tiled and reconstructed if a

RGC's dendrites extended out of field. Dendrites were traced using ImageJ/FIJI and the Simple Neurite Tracer plugin (Longair et al., 2011; Schindelin et al., 2012). Linear Sholl analysis was completed using the Sholl analysis plugin for ImageJ/FIJI (Ferreira et al., 2014). Sholl analysis data was analyzed as the average number of intersections observed in radii bins of 30µm. Data was preprocessed using R 3.3.1 (https://cran.r-project.org/).

iDISCO: For whole mount staining and clearing we use the enhanced version of iDISCO. For a full description of the protocol see (Renier et al., 2014; Renier et al., 2016) and website, *http://lab.rockefeller.edu/tessier-lavigne/assets/file/whole-mount-staining-bench-protocol-january-2015.pdf.* Dissected optic nerves were dehydrated with a methanol/PBS series, 20%, 40%, 60%, 80% and 100%, bleached overnight with 5% H_2O_2 in 100% methanol at 4°C. Rehydrated with a methanol series in PBS and 0.2% TritonX-100, 80%, 60%, 40%, 20%, 0%. Incubated with 1xPBS/0.2%TritonX-100/20%DMSO/0.3Mglycine, 37°C for 2 days. Block in 1xPBS/0.2%TritonX-100/10%DMSO/6% Donkey Serum, 37°C, for 2 days. Wash in 1xPBS/0.2%Tween-20 with 10 ug/ml heparin (PTwH), RT for 1 hour, twice. Incubate with a chicken IgY recognizing GFP epitopes (Aves, #GFP-1020, 1:200) in PTwH/5%DMSO/3% Donkey Serum, 37°C, for 2 days. Wash in PTwH for 10 min, 15 min, 30 min, 1 hour then 2 hours or longer to the next day. Incubate with a Goat anti-chicken Alexa-488 1:300 (ThermoFisher, A-11039) in PTwH/3% Donkey Serum, 37°, 2 days. Wash in PTwH for 10, 15, 30, 60 minutes each and then 2 hours or longer for 2 days. After the final wash the samples were cleared.

Clearing: Washed samples were incubated at room temperature with shaking. First for 1 hour for each step with 20%, 40%, 60%, 80% methanol in water followed by 30 minutes in 100% methanol twice. Next, they were incubated for 3 hours in 66% DiChloroMethane (DCM)/33%

methanol then 20 minutes in 100% DCM, twice. Final clearing solution was in DiBenzylEther (DBE) with no shaking. Cleared optic nerves were mounted onto a cover glass with DBE and imaged on an Olympus confocal microscope (Fluoview 1000) using a 20x UPlanSApo objective (N.A.=0.75). We used an optical zoom of 1.4x and each optic section was 1-1.2 µm. Individual stacks of images were stitched using the program XuvStitch 1.8.099x64 (http://www.xuvtools.org/doku.php).

Axon Analysis: Reconstructed confocal images were analyzed using the FilamentTracer function in Imaris 8.4.1 (Bitplane). To be included in quantitative analysis an axon had to be traced from the proximal optic nerve head to its termination. An axon also had to be resolvable from surrounding axons. FilamentTracer statistics were exported and preprocessed using R 3.3.1 (https://cran.r-project.org/).

Statistical Analysis: Data preprocessing was carried out using R 3.3.1 (https://cran.r-project.org/). Statistical analysis and graph creation was performed with Prism 6 (GraphPad Software, Inc.). See Table 1 for the list of statistical tests used.

Results

Thy1-H Mouse Sparsely Labels Subpopulation of αRGCs

To visualize and track the growth of individual axons in the unsectioned mouse optic nerve we used the Thy1-H-YFP transgenic mouse line, which sparsely labels RGCs, including the regeneration competent αRGCs. (Feng et al., 2000; Coombs et al., 2006; Duan et al., 2015). We observed that there are approximately 70 YFP^+ RGCs in each flat-mounted retina of an adult Thy1-H-YFP mouse (*n=9 retina*). While the number of YFP^+ RGCs per retina varies between animals ($\sigma = 21$), there is a strong correlation ($R^2 = 0.9943$, $p < 0.05$, *n=3 pairs of retina*)

between the left and right retina of an animal. To determine what portion of these YFP^+ RGCs are αRGCs, we immunostained the retinas with an antibody against osteopontin (OSPN), a molecular marker of αRGCs (Duan et al., 2015; Sanes and Masland, 2015). We found that about 70% of YFP^+ RGCs are immunoreactive for OSPN (Figure 1). To further define the molecular identity of YFP^+ RGCs, we stained the retinas with antibodies against melanopsin (OPN4, a marker of intrinsically photosensitive RGCs) and cocaine- and amphetamine-regulated transcript (CART, a marker of direction selective RGCs). Very few YFP^+ RGCs were immunoreactive for OPN4 (i.e. less than 2% of total YFP^+ RGCs) or CART (i.e. less than 10% of total YFP^+ RGCs) (Figure 1A-G). Taken together, these results demonstrate that the Thy1-H-YFP mouse line sparsely labels RGCs, which are primarily $OSPN^+$.

To examine the fate of YFP^+ RGCs in response to axon injury, we performed intraorbital optic nerve crush and evaluated their survival in the presence or absence of a growth promoting factor (Figure 2A-H, J). Six weeks post-crush (6wpc), approximately 13 YFP^+ RGCs survived (Figure 2J; "6wpc"). Of these, about 10 were $OSPN^+$ RGCs, which represents about 76% of total remaining YFP^+ RGCs (Figure 2J). Several studies have shown that virally transferred ciliary neurotrophic factor (CNTF) promotes RGC survival and axon regeneration. AAV2-expressing a secreted form of CNTF did not alter the survival of YFP^+ and $YFP^+/OSPN^+$ RGCs (Figure 2J; "CNTF + 6wpc"). These data show that the majority of surviving YFP^+ RGCs in the Thy1-H-YFP mouse are αRGCs. These findings underscore the utility of the Thy1-H-YFP mouse line for studying axon regeneration in a small number of regeneration competent RGCs, and establishes the feasibility of examining how a specific RGC type will behave after injury and CNTF.

Changes in αRGC Dendrite Morphology Following Axon Injury

In addition to investigating the survival of YFP^+ RGCs, we examined the changes in dendrite morphology following intraorbitral optic nerve crush. Again, we focused on YFP^+ αRGCs (i.e. $YFP^+/OSPN^+$ RGCs). Representative images of $YFP^+/OSPN^+$ RGCs and their dendrites in uninjured and injured ("6wpc") animals are shown in Figure 1D'-F' and Figure 2C-E, I, respectively. At 6 weeks following injury, we did not observe a significant change in dendritic field area or the number of primary dendrites compared to uninjured animals (Figure 2 K, L). Sholl analysis, which is commonly used to evaluate dendritic field arrangement and density (Sholl, 1953), shows that there is a significant reduction in dendrite complexity following intraorbital crush (Figure 2M; "Uninjured vs 6wpc", * $p < 0.05$). AAV-CNTF and crush injury ("CNTF + 6wpc") resulted in RGCs that have fewer primary dendrites and less complex dendritic arbors than injury alone (Figure 2K-M; # $p < 0.05$ "6wpc vs CNTF + 6wpc"; statistically significant difference detected at 30-90 µm radii but no other radii). Thus, these results indicate that acute optic nerve injury leads to reduction in αRGCs' dendritic complexity, and CNTF plus injury causes an even further reduction of dendritic complexity in these neurons.

Immunohistochemical staining of Unsectioned Whole Optic Nerve using iDISCO

To visualize and follow single axons throughout the optic nerve, we subjected adult Thy-H-YFP mouse optic nerves to a tissue clearing procedure which renders tissues transparent and facilitates whole tissue 3D imaging. Since tissue clearing procedures generally reduce endogenous YFP signal, we also immunostained the whole nerves using an antibody against YFP prior to tissue clearing using the iDISCO technique Representative images of uninjured optic nerve subjected to iDISCO and whole tissue imaging are shown in Figure 3A-E. Sparsely labeled individual YFP^+ RGC axons are clearly visible. These axons project linearly from the optic disk to the distal optic nerve. In rare occasions, we also noticed that some axons have a short, rapidly

terminating branch (Figure 3F, G). We also observed occasional YFP^+ cells and their processes in the optic nerve. These are likely astrocytes based on their morphology (Figure 4D, 5A; AC (yellow)). We have established the use of iDISCO to visualize the entire course of Thy1-H-YFP RGC axons through the optic nerve.

Next, we used iDISCO to evaluate how individual axons within a defined population of RGCs regenerate. To determine the validity of our method, we compared the number of RGCs to the number of axons in the optic nerve for 5 animals. Consistent with the number of YFP^+ RGCs in the retina, there were about 70 axons in each nerve. Furthermore, we find a strong correlation between the number of RGCs and axons ($R^2 = 0.9975$, $p < 0.0001$, *n=5 retina, optic nerve pairs*) (Figure 3H), and on average we identified 98.5% of the axons predicted by the number of YFP^+ RGCs. These data indicate that we can identify all YFP+ axons within the optic nerve.

Analysis of Single YFP^+ RGC Axons following Optic Nerve Injury

To examine the morphology and growth pattern of YFP^+ RGC axons following crush injury, first we collected Thy1-H-YFP mouse optic nerves 3 days post-crush ("3dpc") and performed iDISCO and 3D confocal imaging (Figure 4B-C). To determine how an individual axon regenerates, we traced entire axons of some RGCs (Figure 4B-C). Additionally, to visualize all RGC axons, cholera toxin beta (CTB) conjugated to Alexa-594 was injected one hour after crush to label axons anterogradely. Even at this early stage (i.e. 3dpc, Figure 4C, *n=4*), some axons regrew within a small area near the cut end. However, there were no axons beyond the lesion site. Axons in the animals subjected to AAV-CNTF and crush injury ("CNTF + 3dpc", *n=4*) appear similar at this time point (Figure 4B). Disconnected YFP^+ axons which have not yet undergone Wallerian degeneration are visible distal to the lesion site (Figure 4B and C; arrows indicate disconnected bulbs). All YFP^+ axons are clearly disconnected, and no CTB labelled axons are

found far distal to the lesion site (i.e. 1 mm distal to lesion site), strongly indicating that the injury is complete and no axons are spared from axotomy. These results show that some YFP^+ axons begin growing soon after injury (3 days post crush). Notably, this initial growth appears independent to the presence of CNTF.

Second, we observed the growth pattern of YFP^+ axons at an intermediate time-point. At 3 weeks after crush YFP^+ axons in AAV-CNTF treated animals ("CNTF + 3wpc", *n=4 animals*) regrew within regions proximal to the lesion site, forming complex branched and looped structures. Some axons also grew past the lesion site (Figure 4D).

To further investigate this complex growth pattern, we examined axon regeneration at 6 weeks after injury. Optic nerves from 4 individual animals ("6wpc 1-4") are shown in Figure 5. At 6 weeks post-injury (6wpc), nearly all surviving YFP^+ RGC axons were limited to the region proximal to crush site, consistent with the limited ability of CNS axons to regenerate beyond the injury site. We note that the proximal edge of the lesion site occurs at about 1 mm (± 0.2 mm) away from the optic disk. In one animal, we observed one YPF^+ axon past the lesion site, elongating to about 1 mm away from the lesion site (Figure 5A; "6wpc 4"). However, we did not observe regenerating YFP^+ RGC axons far beyond the lesion site (i.e. 3 mm from the lesion), indicating that the crush injury was complete and did not leave axons spared.

Finally, we examined the response of YFP^+ RGC axons 6 weeks following optic nerve crush when the animals received AAV-CNTF injection. Previous studies have demonstrated that CNTF allows some RGC axons to regenerate long distances in the optic nerve with some axons reaching the brain (Pernet et al., 2013; Yungher et al., 2015). We injected AAV-CNTF 3 days before unilateral crush and we collected Thy1-H-YFP mouse optic nerves at 6 weeks after injury. Injured optic nerves from 4 individual animals are shown in Figure 6A, and 7. Three of the 4

animals ("CNTF + 6wpc 1-3") had axons that could be traced in their entirety. The fourth had extensive aberrant growth that prevented the tracing of each axon with certainty (see "CNTF + 6wpc 4" in Figure 7B); however, many axon segments could be traced effectively.

Tracing each axon in its entirety allows comprehensive axon pattern analysis. We observed that axon branching occurs frequently following crush. Approximately half of the axons have 1 or more branches (Figure 6B; "6wpc"). AAV-CNTF significantly increased the number of axons with branches ($p < 0.05$) and the number of branches per axon ($p = 0.0001$, Figure 6B; "6wpc vs CNTF + 6wpc"). Next, we sought to characterize for each axon i) total axon length, ii) how far centrally an axon reached (maximum distance achieved from the optic disk), and iii) how much aberrant growth occurred (aberrant growth = axon total length – maximum distance achieved) (Figure 6C-E). Given that the proximal edge of the crush site is about 1 mm from the optic disk, we see that most axons in the injury control animals remain within or near the lesion site (i.e. within 0.8 mm-1.2 mm from the optic disk). Surprisingly, even in the absence of growth promoting factors many of these axons grew (Figures 5B, 6C). This growth was mostly within the region proximal to the crush. Some axons grew between 1-2 mm in length. This growth consists of branches and loops, growth that does not extend the axon distally along the optic nerve (Figure 5B, 6E). Together, these results show that YFP^+ RGCs are innately capable of re-growing long axons, however these axons are unable to successfully traverse the lesion.

Consistent with the regeneration promoting effects of CNTF, axons grew significantly longer than controls (Figure 6C; $p < 0.001$). Like the injured control animals, many axons failed to grow through the lesion site, and most regrowth was aberrant (Figure 6E). In CNTF animals, the axon length measurement shows that despite growing more than 4-5 mm, some axons are restricted to the lesion area. Independent of treatment, the maximum distance along the optic

nerve most growing axons achieve is associated with the lesion site, around 1000µm from the optic disc (Figure 6D; distance of lesion site from optic disc indicated as horizontal reference line at 1000µm). In fact, the median maximum distance achieved by axons in CNTF animals was only 25% longer than that of the control injured animals despite the fact that the CNTF axons grew 3-4 fold longer in total length (Figure 6C-E). Figure 7A shows reconstructed axons of the "CNTF + 6wpc 3" optic nerve from different viewing angles. This pattern of regrowth was also evident in the fourth animal (Figure 7B; "CNTF + 6wpc 4"). While we were unable to trace each axon from the optic nerve head to termination, we determined that no more than 3 axons grew beyond the lesion site (Figure 7B; arrowheads). As shown in the cross view of the optic nerve (Figure 7, images in the right panels), some axons wrap around the nerve several rounds, further illustrating the extensiveness of tortuous growth.

Discussion

RGCs of different subtypes are connected to distinct presynaptic partners and exhibit an array of responses to visual stimuli. RGCs of different subtypes also project their axons to different brain targets and contribute to image-forming functions as well as non-imaging forming functions (Sanes and Masland, 2015) Anatomically, how do the dendrites and axons of specific RGC types respond to axotomy, as well as after treatments with factors that stimulate axon growth? In the retina, several studies have characterized RGC type-specific changes in dendrite morphology after traumatic axotomy or in glaucoma models. As such, changes in dendrites after insult have been described to some extent. However, the abilities of specific RGC types to regenerate axons and correctly find their targets in adult mammals are just beginning to be determined. Since some studies have shown that many regenerating RGC axons grow circuitously near the lesion and fail to regenerate far, we sought to combine sparse neuronal labeling with iDISCO and follow

individual axons derived primarily from one RGC type; αRGC. The major observations in this study are; 1) αRGC dendrites decrease their complexity following axotomy, and this response to axotomy is exacerbated by CNTF treatment, 2) YPF$^+$ RGC axons grow over unexpectedly long distances before the lesion site with only a few axons being able to successfully traverse the lesion, and 3) YFP$^+$ axons that do regenerate beyond the lesion site elongate aberrantly, form many collateral axons in the optic nerve and fail to reach the brain.

Considerations for Cell Types of Origin of the YFP$^+$ Processes

Our results show that the majority of surviving YFP$^+$ RGCs after injury are immunoreactive for OSPN, indicating that most of these YFP$^+$ RGCs belong to αRGCs (Duan et al., 2015; Sanes and Masland, 2015). Together with the observation that αRGCs have higher capacity to regenerate axons compared to other RGCs in general (Watanabe and Fukuda, 2002; Duan et al., 2015), we reason that the majority of YFP$^+$ RGC axons that we analyzed are likely to be of αRGCs. However, because 24% of surviving RGCs are OSPN-negative (i.e. of the 13 surviving YFP$^+$ RGCs per retina, 10 are YFP$^+$/OSPN$^+$ and 3 are YFP$^+$/OSPN$^-$), we are unable to conclusively determine if the axons that grew beyond the lesion site are of αRGC origin.

Changes in αRGC Dendrites in Responses to Axotomy and CNTF

Using transgenic mice that label defined RGC types, previous studies have examined the morphological changes that occur in RGC dendrites. In a mouse glaucoma model, OFF transient RGCs showed decreased dendritic arborization (Della Santina et al., 2013). Similarly, the dendritic complexity of transient OFF αRGCs from glaucomatous mouse eyes is reduced (El-Danaf and Huberman, 2015). Thus, the results in our study showing loss of dendritic complexity in αRGCs are in line with these previous reports. In contrast, in adult rats, peripheral nerve graft

and AAV-CNTF cause an increase in soma size of RGCs without affecting the dendritic complexity or field size (Rodger et al., 2012). However, when examined specifically in the RGC 1 subtype (i.e. RGCs with a large soma), AAV-CNTF caused a significant reduction in the complexity of the dendritic arbors, again without reducing the field size (Rodger et al., 2012). In line with the previous study, our results show that AAV-CNTF leads to a significant decrease in arbor complexity without altering the dendritic field size in most cells. Thus, our results suggest that while αRGC axons are highly regenerative and quite likely generate complex arbors (i.e. in response to CNTF), their dendrites become less complex. In this regard, one could ask why and how does CNTF cause even greater reduction in dendrite complexity in these RGCs? The molecular and cellular mechanisms underlying such different behaviors by the axons and dendrites are unknown. It is also unclear whether the reduction in dendrite arbor complexity will be potentially disruptive for the function of these RGCs (i.e. receive less input from their presynaptic partners). These are interesting questions that may deserve further investigation.

We observed that the majority of YFP-labelled αRGCs (~80%) in this experimental example died at 6 weeks after injury. Currently, it is unclear whether these YFP^+ αRGCs die long after injury because of lack of intrinsic survival signals or because they are disconnected for a long time and lack trophic support from the target. It is also possible that they die because they remain unmyelinated (i.e. not remyelinated) for a long period time, lacking the survival signal(s) and other type(s) of support from the oligodendrocytes (or even astrocytes). The question why most RGCs die remains nebulous and justifies further investigation.

Highly Regenerative Yet Unable to Go Far

Several prior studies have adopted tissue clearing strategies and examined axon regeneration in unsectioned, whole CNS tissues (Erturk et al., 2011; Laskowski and Bradke, 2013; Luo et al.,

2013; Pernet et al., 2013; Soderblom et al., 2015). In this study, we sought to expand the 3D analysis to track single axons in given neuronal types. To our knowledge, our study is the first to report the adaptation of sparse labeling and whole tissue staining to attain the entire projection profiles of regenerating axons. Perhaps the most striking observation in our study was the extensive and circuitous regeneration of RGC axons occurring proximal to the lesion site. Axons start to penetrate through the lesion, sometime more than once, but each time they turn back towards the retina and thus they elongate within the proximal optic nerve region (i.e. near the optic nerve head). Additionally, axons that surpass the lesion continue to branch and misroute, with these events lacking an obvious spatial pattern (e.g. occurring near the lesion site). We also note that none of these axons grew past the optic chiasm. As can be seen in Figures 4-7, regenerating axons stop at different distances away from the chiasm. Previous studies have suggested that optic chiasm may inhibit or halt some axons to grow further (Luo et al., 2013; Crair and Mason, 2016). At least for these neurons however, the reason that they fail to grow past the chiasm does not seem to be due to chiasmatic barrier as these axons terminate or turn towards the eye even before they get close to the optic chiasm.

How does an axon successfully traverse the lesion? In the CNS lesion, various growth inhibitory molecules are present. Molecular barriers within the lesion area include chondroitin sulfate proteoglycans and myelin-associated inhibitors (Yiu and He, 2006). Astrocytes and fibroblasts interact to establish a scar, surrounding the lesion. Therefore, to successfully traverse the lesion, a growing axon will need to modify the extracellular matrix (ECM) and overcome inhibitory/repulsive cues. Differential expression of ECM modifying enzymes and cell surface receptors may explain why some axons never cross the lesion while others do. This simple explanation is challenged by our finding that axons proximal to the lesion form extensive

branches and loops and then eventually grow through the lesion (i.e. see Figure 6A; "CNTF + 6wpc 1"). For this to occur, axons would need to be dynamically responsive to their environment and alter gene expression accordingly (i.e. after failing to traverse the lesion, they change expression of certain molecules to better suit the lesion environment), or crossing the lesion site is a stochastic event. Future investigation will be needed to identify if specific RGCs are can cross the lesion barrier, and what interventions can help axons through this environment.

The tracing of individual axons allowed us to measure the total length of individual axons as well as the maximum distances from the eye. Unequivocally, we find that while many axons travel long distances, their circuitous growth results in them remaining within close vicinity to the lesion site. The observation that the regenerating axons grow aberrantly within the optic nerve is mostly in agreement with previous studies (Luo et al., 2013; Pernet et al., 2013). Nonetheless, our current study provides a complete picture of individual axon trajectory, from their entry into the optic nerve to the end of their route. This is particularly the case for the portion of axons located in the proximal area to the injury site which was not possible in the previous studies that have used CTB as a tracer for all RGC axons. Overall, our results build upon prior studies and further show that the growth of YFP^+ RGCs axons are tortuous in their paths, and that these axons are unlikely to re-innervate their brain targets after CNTF treatment.

Question of Treatment and Cell Type-Specific Axon Behaviors

CNTF is only one of many factors that can induce axon regeneration. Do different regeneration stimulating factors cause a similar degree of aberrant growth and misrouting? Do the axons of all RGC types have similar propensity to misroute? Studies by Lim et al., and De Lima et al., showed that at least under certain conditions, some RGC axons are able to regenerate with minimal misrouting and back to their correct targets (de Lima et al., 2012; Lim et al., 2016). In

some instances, these RGC axons seem to travel linearly towards the brain (Lim et al., 2016). It appears that under some conditions, RGC axons may be able to navigate through the injured optic nerve. It is unknown what molecular and cellular factors minimize misrouting and produce directed growth within the optic nerve and beyond. It may be interesting to apply 3D analysis and examine the behavior of αRGCs and other RGC types under additional growth-promoting conditions. This could help determine whether the aberrant growth seen in the present study is specific to some RGC types or to CNTF treatment *per se*.

It is known that certain types of neurons in different CNS regions including the supraspinal serotonergic neurons are able to spontaneously remodel and re-extend axons after axotomy (Hawthorne et al., 2011). On the other hand, other neurons including the corticospinal tract axons are strongly refractory to regeneration where the cut dystrophic axons regress with virtually no signs of regrowth (Thallmair et al., 1998; Liu et al., 2010). In the case of RGCs, we know from studies using CTB tracing that a few of these neurons can spontaneously regrow axons, at least to some short distance into the lesion. The lengthy axons seen even without CNTF in our study indicate that RGCs (and perhaps other CNS neurons) may have much higher growth capacity than generally thought. In the case of peripheral neurons, the dorsal root ganglion (DRG) axons send collaterals and misroute following injury to the central branch (Kerschensteiner et al., 2005). It would be interesting to determine if this aberrant growth of DRG axons is amplified following pre-conditioning injury, a method to promote regeneration of a DRG's central branch.

These findings highlight the need for prudence when evaluating a growth factor to promote axon regeneration. CNTF and other growth factors are frequently used in regeneration studies to stimulate axon growth. In our study, CNTF produced abundant axon growth, but this growth was highly aberrant. Thus, this growth factor caused "too much of a good thing". Therefore, future

treatments must be adjusted to maximize axon growth into brain targets, and minimize axon branching and tortuous growth.

Overall, our study documents the morphological changes that occur in αRGCs after optic nerve injury. Tracking the entire paths of individual axons reveal that these RGCs can naturally re-extend axons extremely well, but both their inability to traverse the lesion area and their circuitous axon growth limit reconnection with the brain. Our results counter the general view that RGC axons are incapable of lengthy regeneration, and shift the focus from promoting axon elongation, to understanding factors that prevent direct growth of axons through the injured nerve.

References

Belin S, Nawabi H, Wang C, Tang S, Latremoliere A, Warren P, Schorle H, Uncu C, Woolf CJ, He Z, Steen JA (2015) Injury-induced decline of intrinsic regenerative ability revealed by quantitative proteomics. Neuron 86:1000-1014.

Coombs J, van der List D, Wang GY, Chalupa LM (2006) Morphological properties of mouse retinal ganglion cells. Neuroscience 140:123-136.

Crair MC, Mason CA (2016) Reconnecting Eye to Brain. J Neurosci 36:10707-10722.

de Lima S, Koriyama Y, Kurimoto T, Oliveira JT, Yin Y, Li Y, Gilbert HY, Fagiolini M, Martinez AM, Benowitz L (2012) Full-length axon regeneration in the adult mouse optic nerve and partial recovery of simple visual behaviors. Proc Natl Acad Sci U S A 109:9149-9154.

Della Santina L, Inman DM, Lupien CB, Horner PJ, Wong RO (2013) Differential progression of structural and functional alterations in distinct retinal ganglion cell types in a mouse model of glaucoma. J Neurosci 33:17444-17457.

Duan X, Qiao M, Bei F, Kim IJ, He Z, Sanes JR (2015) Subtype-specific regeneration of retinal ganglion cells following axotomy: effects of osteopontin and mTOR signaling. Neuron 85:1244-1256.

El-Danaf RN, Huberman AD (2015) Characteristic patterns of dendritic remodeling in early-stage glaucoma: evidence from genetically identified retinal ganglion cell types. J Neurosci 35:2329-2343.

Erturk A, Mauch CP, Hellal F, Forstner F, Keck T, Becker K, Jahrling N, Steffens H, Richter M, Hubener M, Kramer E, Kirchhoff F, Dodt HU, Bradke F (2011) Three-dimensional imaging of the unsectioned adult spinal cord to assess axon regeneration and glial responses after injury. Nat Med 18:166-171.

Feng G, Mellor RH, Bernstein M, Keller-Peck C, Nguyen QT, Wallace M, Nerbonne JM, Lichtman JW, Sanes JR (2000) Imaging neuronal subsets in transgenic mice expressing multiple spectral variants of GFP. Neuron 28:41-51.

Ferreira TA, Blackman AV, Oyrer J, Jayabal S, Chung AJ, Watt AJ, Sjostrom PJ, van Meyel DJ (2014) Neuronal morphometry directly from bitmap images. Nat Methods 11:982-984.

Hawthorne AL, Hu H, Kundu B, Steinmetz MP, Wylie CJ, Deneris ES, Silver J (2011) The unusual response of serotonergic neurons after CNS Injury: lack of axonal dieback and enhanced sprouting within the inhibitory environment of the glial scar. J Neurosci 31:5605-5616.

Kerschensteiner M, Schwab ME, Lichtman JW, Misgeld T (2005) In vivo imaging of axonal degeneration and regeneration in the injured spinal cord. Nat Med 11:572-577.

Laskowski CJ, Bradke F (2013) In vivo imaging: a dynamic imaging approach to study spinal cord regeneration. Exp Neurol 242:11-17.

Leibinger M, Andreadaki A, Gobrecht P, Levin E, Diekmann H, Fischer D (2016) Boosting Central Nervous System Axon Regeneration by Circumventing Limitations of Natural Cytokine Signaling. Mol Ther 24:1712-1725.

Lim JH, Stafford BK, Nguyen PL, Lien BV, Wang C, Zukor K, He Z, Huberman AD (2016) Neural activity promotes long-distance, target-specific regeneration of adult retinal axons. Nat Neurosci 19:1073-1084.

Lin B, Wang SW, Masland RH (2004) Retinal ganglion cell type, size, and spacing can be specified independent of homotypic dendritic contacts. Neuron 43:475-485.

Liu K, Lu Y, Lee JK, Samara R, Willenberg R, Sears-Kraxberger I, Tedeschi A, Park KK, Jin D, Cai B, Xu B, Connolly L, Steward O, Zheng B, He Z (2010) PTEN deletion enhances the regenerative ability of adult corticospinal neurons. Nat Neurosci 13:1075-1081.

Longair MH, Baker DA, Armstrong JD (2011) Simple Neurite Tracer: open source software for reconstruction, visualization and analysis of neuronal processes. Bioinformatics 27:2453-2454.

Luo X, Salgueiro Y, Beckerman SR, Lemmon VP, Tsoulfas P, Park KK (2013) Three-dimensional evaluation of retinal ganglion cell axon regeneration and pathfinding in whole mouse tissue after injury. Exp Neurol 247:653-662.

Mehta ST, Luo X, Park KK, Bixby JL, Lemmon VP (2016) Hyperactivated Stat3 boosts axon regeneration in the CNS. Exp Neurol 280:115-120.

Moore DL, Blackmore MG, Hu Y, Kaestner KH, Bixby JL, Lemmon VP, Goldberg JL (2009) KLF family members regulate intrinsic axon regeneration ability. Science 326:298-301.

Nawabi H, Belin S, Cartoni R, Williams PR, Wang C, Latremoliere A, Wang X, Zhu J, Taub DG, Fu X, Yu B, Gu X, Woolf CJ, Liu JS, Gabel CV, Steen JA, He Z (2015) Doublecortin-Like Kinases Promote Neuronal Survival and Induce Growth Cone Reformation via Distinct Mechanisms. Neuron 88:704-719.

Park KK, Liu K, Hu Y, Smith PD, Wang C, Cai B, Xu B, Connolly L, Kramvis I, Sahin M, He Z (2008) Promoting axon regeneration in the adult CNS by modulation of the PTEN/mTOR pathway. Science 322:963-966.

Pernet V, Joly S, Dalkara D, Jordi N, Schwarz O, Christ F, Schaffer DV, Flannery JG, Schwab ME (2013) Long-distance axonal regeneration induced by CNTF gene transfer is impaired by axonal misguidance in the injured adult optic nerve. Neurobiol Dis 51:202-213.

Puttagunta R, Tedeschi A, Soria MG, Hervera A, Lindner R, Rathore KI, Gaub P, Joshi Y, Nguyen T, Schmandke A, Laskowski CJ, Boutillier AL, Bradke F, Di Giovanni S (2014) PCAF-dependent epigenetic changes promote axonal regeneration in the central nervous system. Nat Commun 5:3527.

Renier N, Wu Z, Simon DJ, Yang J, Ariel P, Tessier-Lavigne M (2014) iDISCO: a simple, rapid method to immunolabel large tissue samples for volume imaging. Cell 159:896-910.

Renier N, Adams EL, Kirst C, Wu Z, Azevedo R, Kohl J, Autry AE, Kadiri L, Umadevi Venkataraju K, Zhou Y, Wang VX, Tang CY, Olsen O, Dulac C, Osten P, Tessier-Lavigne M (2016) Mapping of Brain Activity by Automated Volume Analysis of Immediate Early Genes. Cell 165:1789-1802.

Rodger J, Drummond ES, Hellstrom M, Robertson D, Harvey AR (2012) Long-term gene therapy causes transgene-specific changes in the morphology of regenerating retinal ganglion cells. PLoS One 7:e31061.

Sanes JR, Masland RH (2015) The types of retinal ganglion cells: current status and implications for neuronal classification. Annu Rev Neurosci 38:221-246.

Schindelin J, Arganda-Carreras I, Frise E, Kaynig V, Longair M, Pietzsch T, Preibisch S, Rueden C, Saalfeld S, Schmid B, Tinevez JY, White DJ, Hartenstein V, Eliceiri K, Tomancak P, Cardona A (2012) Fiji: an open-source platform for biological-image analysis. Nat Methods 9:676-682.

Sholl DA (1953) Dendritic organization in the neurons of the visual and motor cortices of the cat. J Anat 87:387-406.

Smith PD, Sun F, Park KK, Cai B, Wang C, Kuwako K, Martinez-Carrasco I, Connolly L, He Z (2009) SOCS3 deletion promotes optic nerve regeneration in vivo. Neuron 64:617-623.

Soderblom C, Lee DH, Dawood A, Carballosa M, Jimena Santamaria A, Benavides FD, Jergova S, Grumbles RM, Thomas CK, Park KK, Guest JD, Lemmon VP, Lee JK, Tsoulfas P (2015) 3D Imaging of Axons in Transparent Spinal Cords from Rodents and Nonhuman Primates. eNeuro 2.

Thallmair M, Metz GA, Z'Graggen WJ, Raineteau O, Kartje GL, Schwab ME (1998) Neurite growth inhibitors restrict plasticity and functional recovery following corticospinal tract lesions. Nat Neurosci 1:124-131.

Watanabe M, Fukuda Y (2002) Survival and axonal regeneration of retinal ganglion cells in adult cats. Prog Retin Eye Res 21:529-553.

Yiu G, He Z (2006) Glial inhibition of CNS axon regeneration. Nat Rev Neurosci 7:617-627.

Yungher BJ, Luo X, Salgueiro Y, Blackmore MG, Park KK (2015) Viral vector-based improvement of optic nerve regeneration: characterization of individual axons' growth patterns and synaptogenesis in a visual target. Gene Ther 22:811-821.

Figure Legends

Figure 1. Identification of RGC subtypes labeled by the Thy1-H-YFP mouse line. Retinal whole mount preparations were immunostained for YFP (green) and markers of three RGC subtypes (magenta): OSPN (osteopontin) (***A, D, and D'***), OPN4 (melanopsin) (***B, E, and E'***), and CART (cocaine- and amphetamine-regulated transcript). (***C, F, and F'***). ***A-C,*** Low magnification images of flat mount retina specimens that demonstrate the number of RGCs labeled by the Thy1-H-YFP mouse line as well as by each RGC subtype marker, scale bar = 500µm. ***D-F***, High magnification images of RGCs labeled by each marker. ***D'-F'***, YFP^+ RGCs (green) shown in the presence of different RGC subtypes (magenta). Arrowheads mark YFP^+ RGCs immunoreactive for subtype marker. Scale bar = 50 µm. ***G,*** The percentage of YFP^+ RGCs that are immunoreactive for each marker. Bar graphs of mean ± SEM, (Retinas: OSPN *n=9*, OPN4 *n=3*, and CART *n = 3*).

Figure 2. Response of YFP^+ RGCs to axonal injury and AAV-CNTF injection. Six weeks following optic nerve crush (6wpc) retinal whole mounts from AAV-PLAP ("6wpc") (***A, C-E***), and AAV-CNTF ("CNTF + 6wpc") injected (***B, F-H***) animals were immunostained for YFP (green) and OSPN (magenta). ***A, B***, Low magnification images of retinal whole mount preparations show few YFP^+ RGCs surviving 6 weeks following crush injury. Scale bar = 500 µm. RGCs were defined by: soma location in the ganglion cell layer or inner nuclear layer (displaced RGC), and the presence of an axon. ***C-H***, High magnification images of $YFP^+/OSPN^+$ RGCs from "6wpc" (***C-E***) and "CNTF + 6wpc" (***F-H***) animals. Three example RGCs are shown for each animal group, scale bar = 50 µm. ***I***, Example traces of $YFP^+/OSPN^+$ RGC dendrites from each condition, scale bar = 50 µm. ***J***, Quantification of YFP^+ RGCs and $YFP^+/OSPN^+$

RGCs in each condition, each dot represents 1 retina ("6wpc" *n = 4*, "CNTF + 6wpc" *n = 5*). ***K***, Number of primary dendrites observed for each RGC. (*p < 0.05 "6wpc" vs "CNTF + 6wpc", ANOVA with Tukey's post hoc*). ***L***, Dendritic field size for each RGC (mm^2). ***J-L***, Bars = median and interquartile range. ***M***, Sholl analysis of RGC dendrites, bars = mean ± SEM (* *p < 0.05 "Uninjured vs 6wpc", § p < 0.05 "Uninjured vs CNTF + 6wpc", # p < 0.05 "6wpc vs CNTF + 6wpc", ANOVA with Tukey's post hoc at each distance*). ***K-M:*** Uninjured n=16 RGCs from 5 animals, "6wpc" n = 15 RGCs from 4 animals, "CNTF + 6wpc" n=15 RGCs from 5 animals).

Figure 3. The iDISCO technique was used to immunostain unsectioned optic nerves from Thy1-H-YFP mice. ***A***, Maximum intensity projection (MIP) image of a full thickness optic nerve showing YFP^+ axons (white). Orientation: Optic nerve head on left, distal towards the optic chiasm to the right. ***B***, Example traces of single YFP^+ axons, each color represents one continuous axon. Color assignment was arbitrary. ***C***, Traces superimposed on MIP image, scale bar = 500µm. ***D, E***, High magnification view of boxed area in **A,** scale bar = 30 µm. ***F,*** Example of an "Uninjured" axon branch. ***G***, Trace overlay of **F**, scale bar = 10 µm, arrowhead = branch point. ***H***, Scatter plot of the number of RGCs counted in the retina (abscissa) vs the number of axons counted in each optic nerve (ordinate) per animal, *n = 5*. Dashed line = linear fit.

Figure 4. iDISCO based 3D analysis of Thy1H-YFP axons following optic nerve crush. ***A,*** Diagram of the eye and optic nerve, indicating the location of intravitreal injection and the site of optic nerve crush. Two RGCs shown in green. Approximate distance of crush site to optic disc, and to optic chiasm are shown. Observed distance *in vivo* may vary ± 0.2mm. ***B-D***, Maximum intensity projection (MIP) images of full thickness optic nerves showing YFP^+ axons (white).

Traces for YFP$^+$ axons are shown with MIP image. Orientation: Optic nerve head on left, distal towards the optic chiasm to the right. ***B***, Intravitreal AAV-CNTF injected optic nerve 3 days post crush ("CNTF + 3dpc"), *n=4*. ***C,*** Optic nerve 3 days post crush (3dpc) (i.e. no AAV-CNTF), *n=4*. ***B and C***, One hour post crush mice received intravitreal injection of cholera toxin beta (CTB)-Alexa 594 (red). Arrows in B and C indicate a disconnected stump of distal degenerating axon. ***D***, Intravitreal AAV-CNTF injected optic nerve 3 weeks post crush ("CNTF + 3wpc"), *n=4*. AC (yellow) marks an example of a presumed astrocyte. ***B-D***, Lesion site indicated by red *. Each color represents an individual axon. Color assignment was arbitrary. Scale bar = 100 µm. Single axon traces are presented for select axons that displayed growth.

Figure 5. iDISCO based 3D analysis of YFP$^+$ axons 6 weeks following optic nerve crush (6wpc). ***A***, Maximum intensity projection (MIP) images of full thickness optic nerves showing YFP$^+$ axons (white). Lesion site indicated by red *. Orientation: Optic nerve head on left, distal towards the optic chiasm to the right. Four optic nerves were members of this group, "6wpc 1-4". Traces for YFP$^+$ axons are shown with MIP image. Each color represents an individual axon. Color assignment was arbitrary. Scale bar = 100 µm. AC (yellow) in "6wpc 2" and "6wpc 3" indicate examples of presumed astrocytes. White # in "6wpc 3": Extraocular muscle that was not completely removed during dissection. ***B***, Three axons from "6wpc 1" and "6wpc 3" are shown. Each axon grows but fails to cross lesion site. Branch points marked by arrowheads. Lesion site indicated by red *

Figure 6. iDISCO based 3D analysis of YFP$^+$ axons 6 weeks following AAV-CNTF injection and optic nerve crush ("CNTF + 6wpc"). ***A***, Maximum intensity projection (MIP) images of full

thickness optic nerves showing YFP^+ axons (white). Lesion site indicated by red *. Orientation: Optic nerve head on left, distal towards the optic chiasm to the right. Four optic nerves were members of this group, "CNTF + 6wpc 1-4". Only animals "CNTF + 6wpc 1-3" had axons that could be fully traced and were included in the quantification. Traces for YFP^+ axons are shown with MIP image. Each color represents an individual axon. Color assignment was arbitrary. Scale bars = 100µm. ***B***, Dot plot of the number of branches occurring per axon in each group, each dot represents one axon. ***C***, Dot plot of axon total length for each axon. ***D***, Dot plot of the maximum distance each axon was found from the retina/optic nerve head boundary. Dashed horizontal reference line indicating lesion site at 1000 µm. ***E***, Dot plot of aberrant growth for each axon. Bars = median and interquartile range. Uninjured n = 34 axons from 3 animals, "6wpc" n = 42 axons from 4 animals, "CNTF + 6wpc" n = 22 axons from 3 animals ("CNTF + 6wpc 1-3").

Figure 7. iDISCO based 3D visualization of aberrant axon growth. **A**, Axon traces from animal "CNTF + 6wpc 3" are shown from 3 perspectives. CNTF + 6wpc 3 and CNTF + 6wpc 3' show longitudinal views of the same optic nerve. CNTF + 6wpc 3'' and CNTF + 6wpc 4''' show coronal views of the optic nerve. ***B***, Animal "CNTF + 6wpc 4". Continuous axon segments that could be traced with a high degree of certainty are shown. Each color represents a continuous segment. Lesion site indicated by red *. Arrowheads mark the three segments that grew beyond the lesion site. Scale bars = 100 µm.

Table 1. Summary of statistics

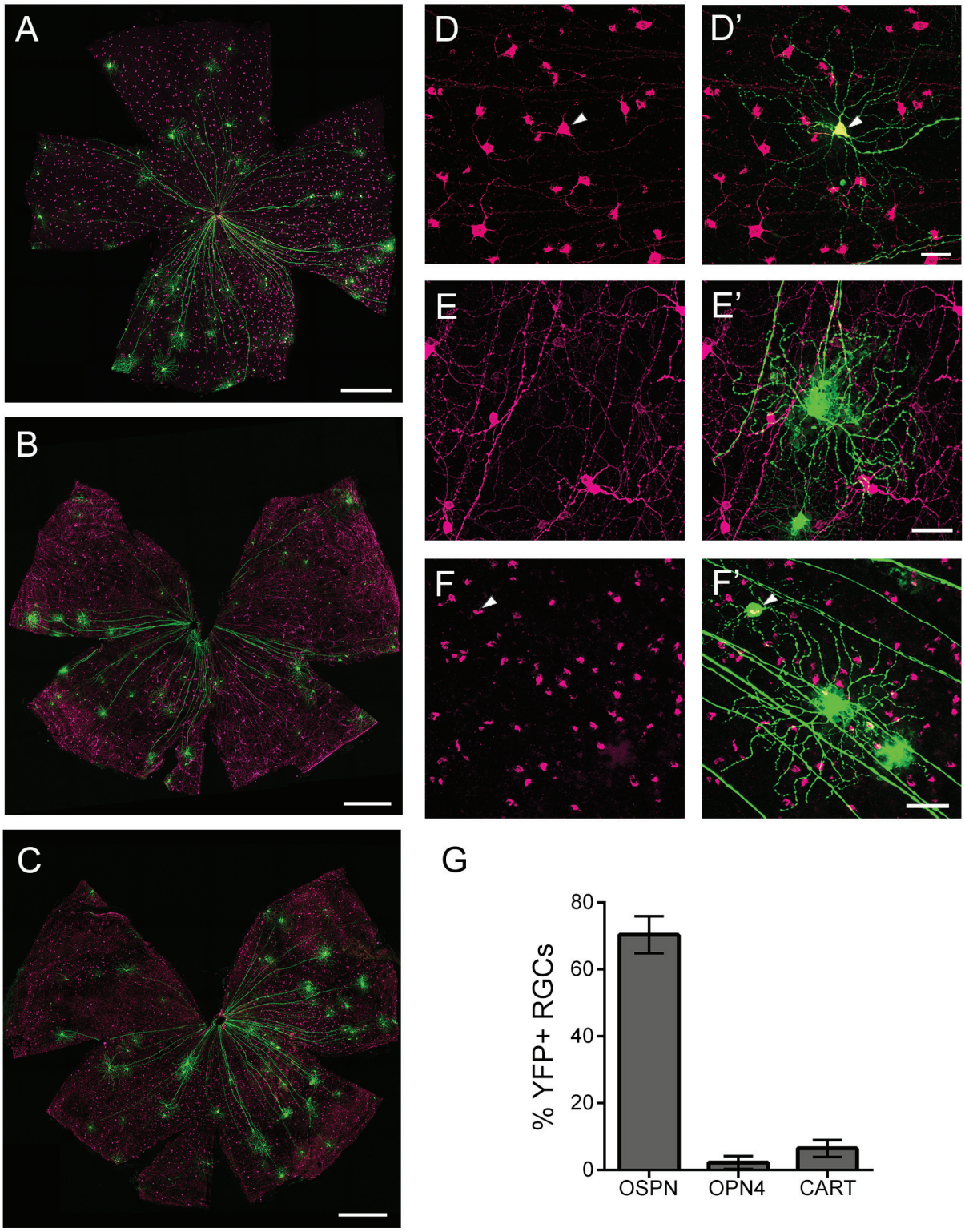

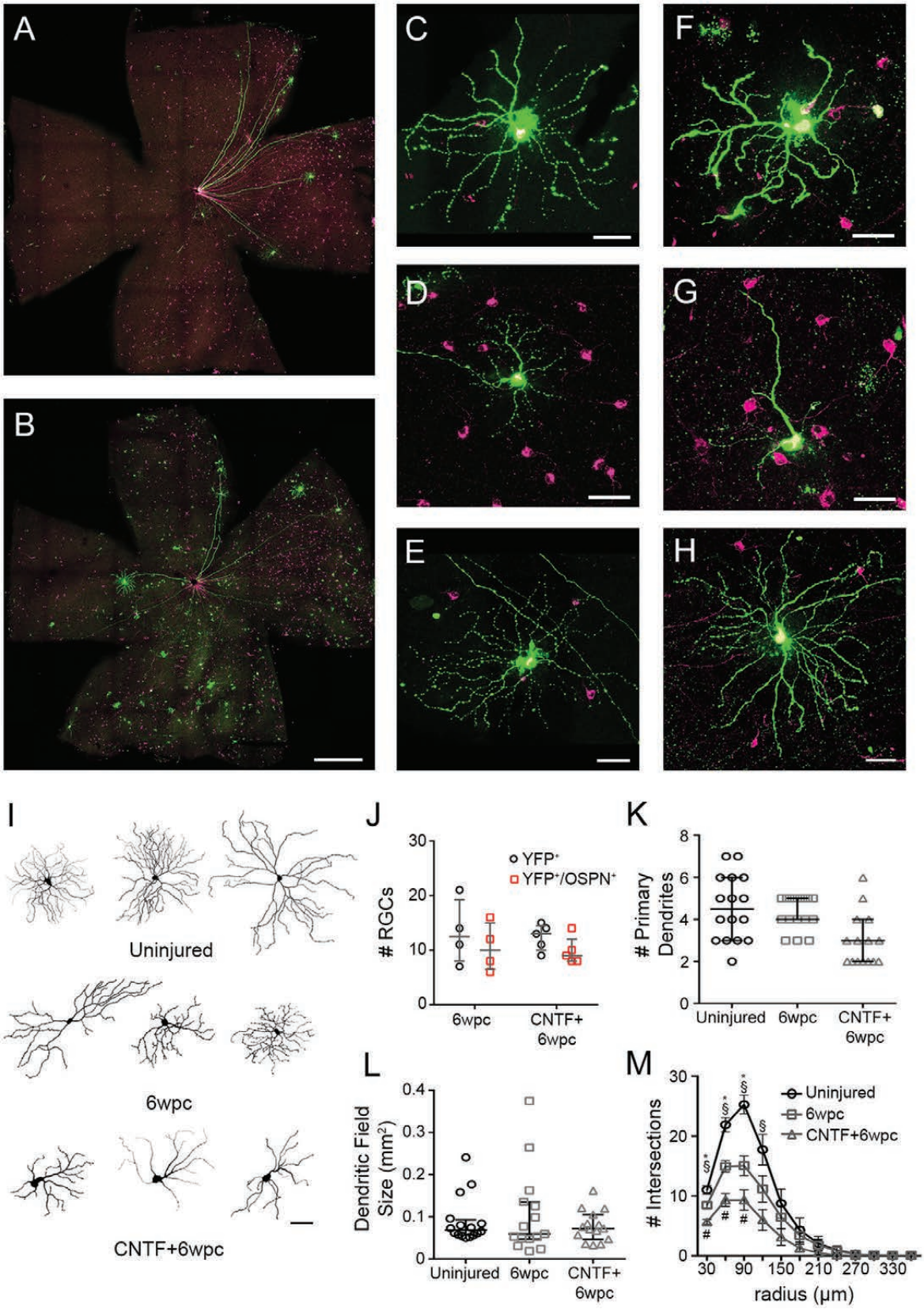

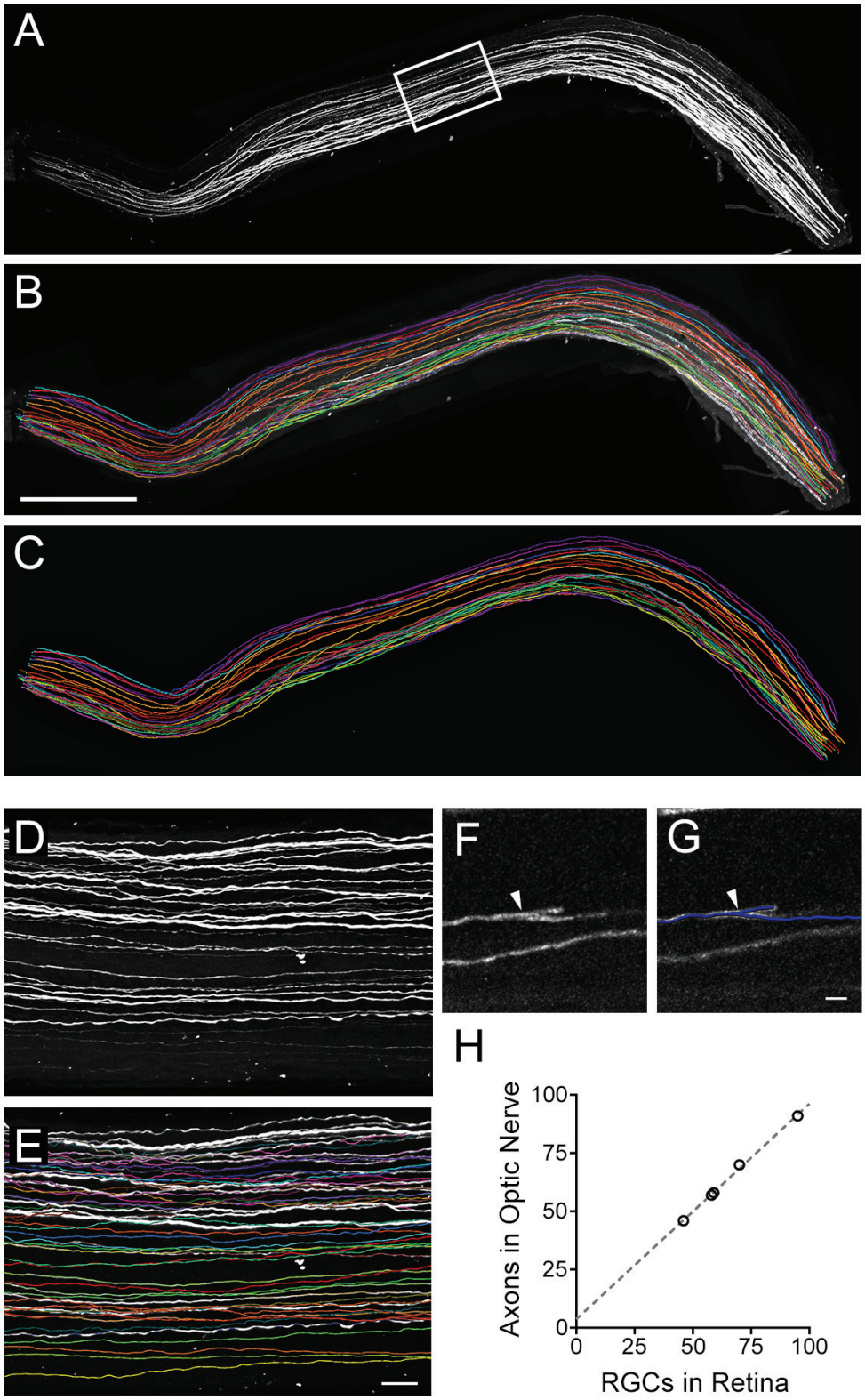

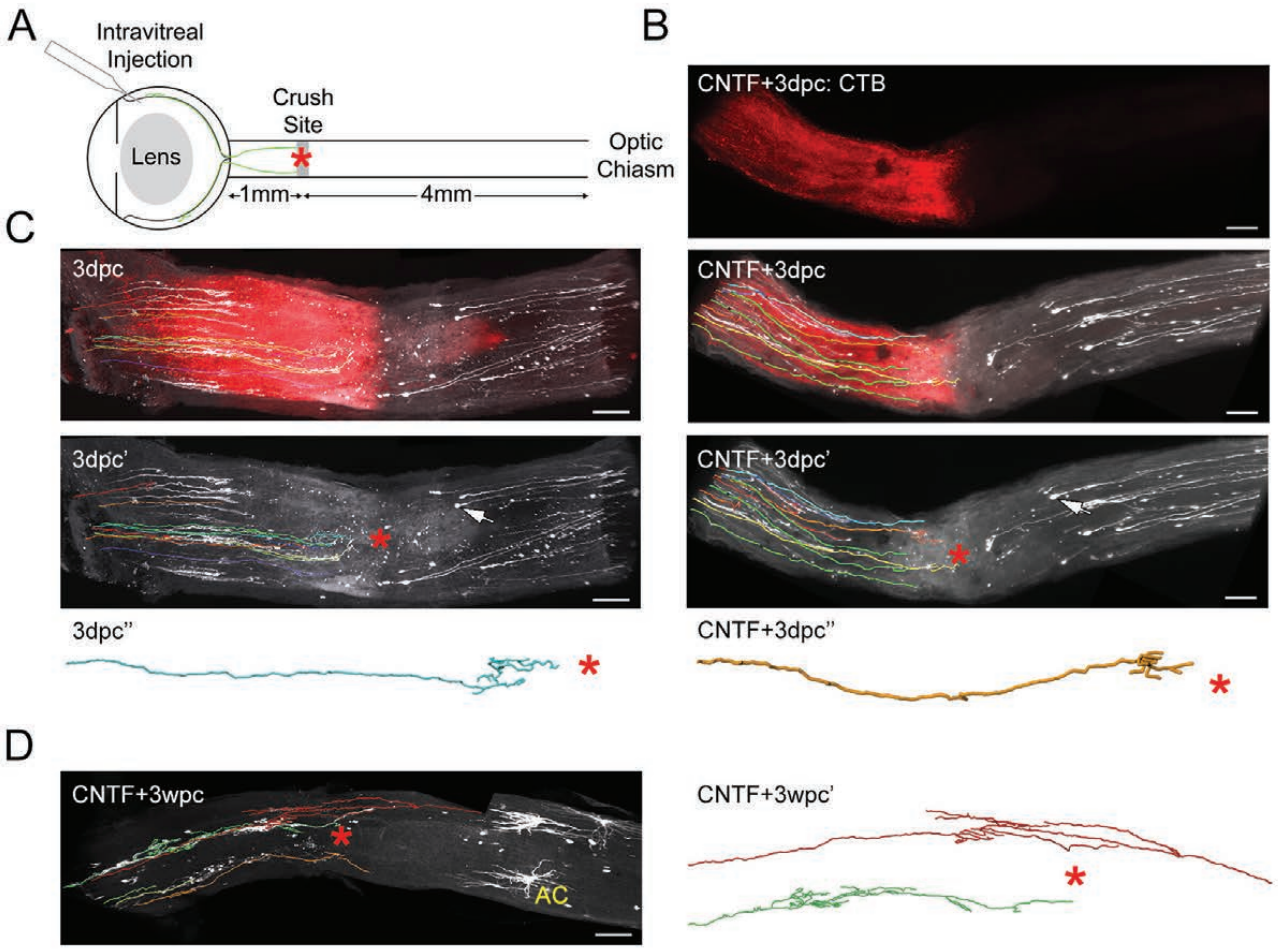

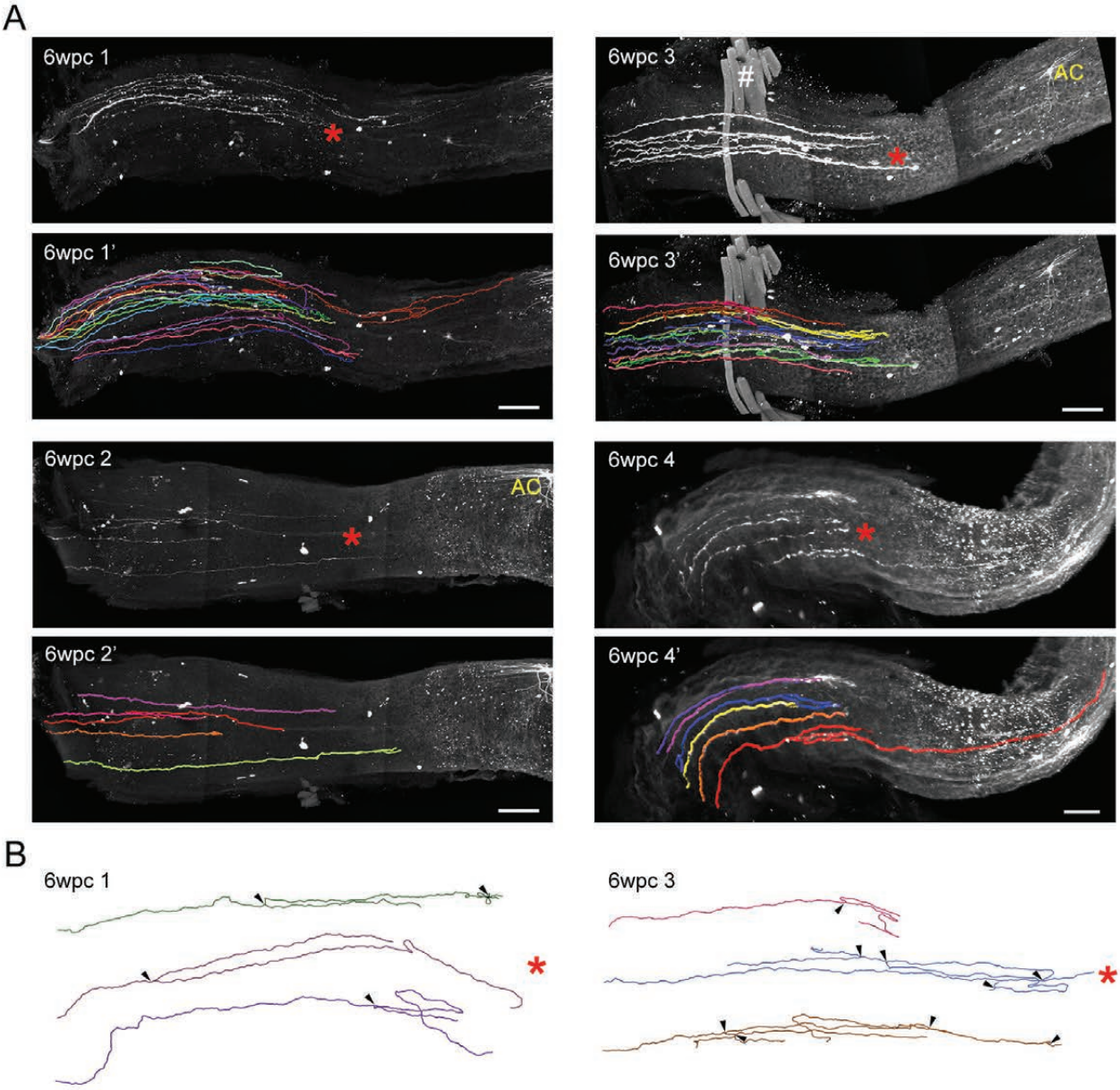

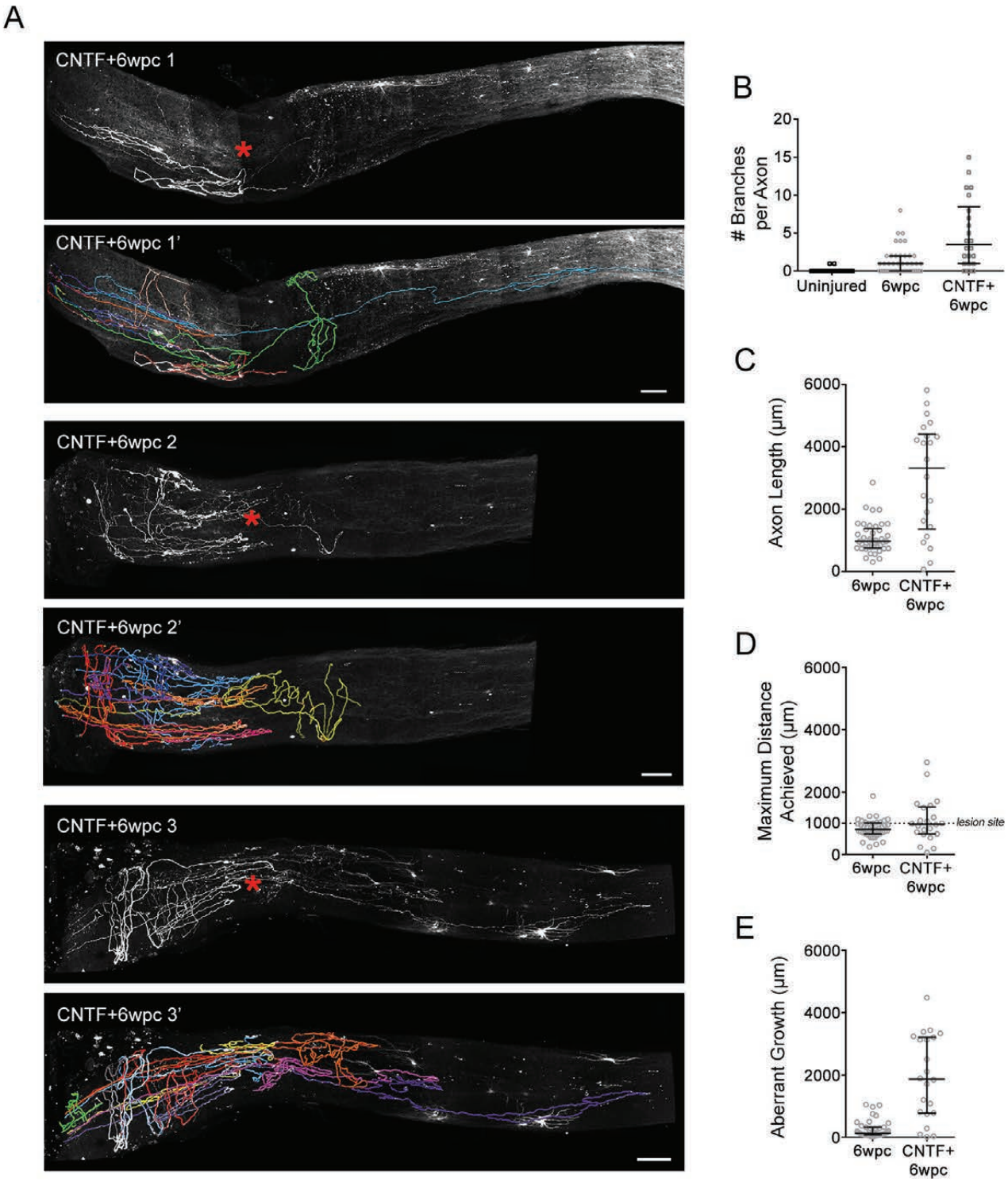

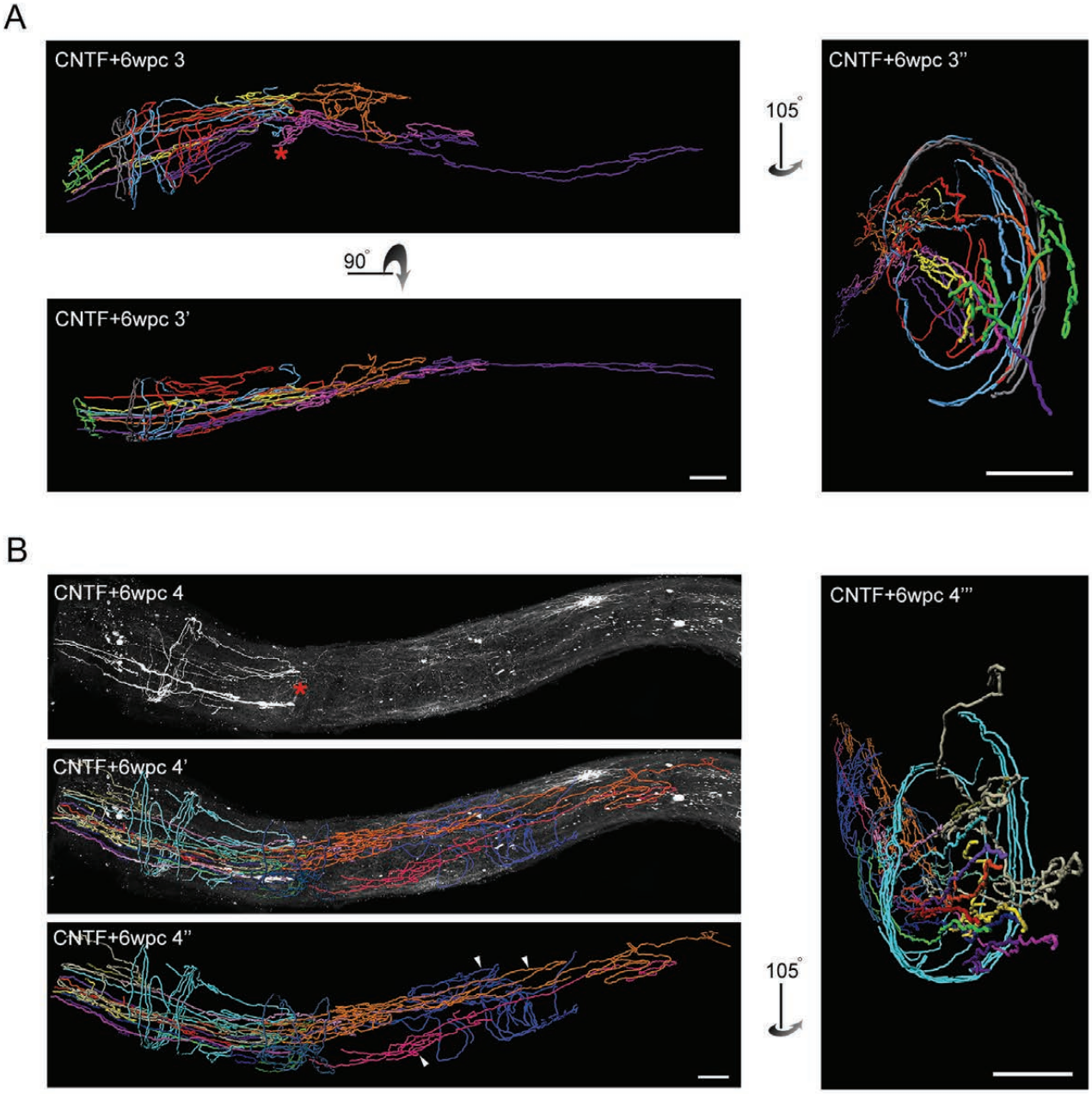

Table 1. Statistical Table

	Data structure	Type of test	Observed Power ($\alpha = 0.05$)
Results text	dependent continuous	Pearson correlation	0.0479
Figure 2K	3 groups, normal distribution	ANOVA	
Uninjured vs 6wpc	normal distribution	post hoc: Tukey's multiple comparisons	0.7877
Uninjured vs CNTF + 6wpc	normal distribution	post hoc: Tukey's multiple comparisons	0.0032
6wpc vs CNTF + 6wpc	normal distribution	post hoc: Tukey's multiple comparisons	0.0214
Figure 2L	3 groups, normal distribution	ANOVA	0.5523
Figure 2M	3 groups, repeated measures, normal distrubtion	2-way ANOVA	
Uninjured vs 6wpc	normal distribution	post hoc: Tukey's multiple comparisons	0.0188
Uninjured vs CNTF + 6wpc	normal distribution	post hoc: Tukey's multiple comparisons	< 0.0001
6wpc vs CNTF + 6wpc	normal distribution	post hoc: Tukey's multiple comparisons	0.0353
Figure 2M (ANOVA at each distance)			
Distance: 30µm	3 groups, normal distribution	ANOVA	
Uninjured vs 6wpc	normal distribution	post hoc: Tukey's multiple comparisons	0.0055
Uninjured vs CNTF + 6wpc	normal distribution	post hoc: Tukey's multiple comparisons	< 0.0001
6wpc vs CNTF + 6wpc	normal distribution	post hoc: Tukey's multiple comparisons	0.0024
Distance: 60µm	3 groups, normal distribution	ANOVA	
Uninjured vs 6wpc	normal distribution	post hoc: Tukey's multiple comparisons	0.0001
Uninjured vs CNTF + 6wpc	normal distribution	post hoc: Tukey's multiple comparisons	< 0.0001
6wpc vs CNTF + 6wpc	normal distribution	post hoc: Tukey's multiple comparisons	0.0019
Distance: 90µm	3 groups, normal distribution	ANOVA	
Uninjured vs 6wpc	normal distribution	post hoc: Tukey's multiple comparisons	0.0002
Uninjured vs CNTF + 6wpc	normal distribution	post hoc: Tukey's	< 0.0001

		multiple comparisons	
6wpc vs CNTF + 6wpc	normal distribution	post hoc: Tukey's multiple comparisons	0.0455
Distance: 120µm	3 groups, normal distribution	ANOVA	
Uninjured vs 6wpc	normal distribution	post hoc: Tukey's multiple comparisons	0.1008
Uninjured vs CNTF + 6wpc	normal distribution	post hoc: Tukey's multiple comparisons	0.0014
6wpc vs CNTF + 6wpc	normal distribution	post hoc: Tukey's multiple comparisons	0.2399
Distance: 150µm	3 groups, normal distribution	ANOVA	
Uninjured vs 6wpc	normal distribution	post hoc: Tukey's multiple comparisons	0.6984
Uninjured vs CNTF + 6wpc	normal distribution	post hoc: Tukey's multiple comparisons	0.1204
6wpc vs CNTF + 6wpc	normal distribution	post hoc: Tukey's multiple comparisons	0.4675
Figure 3H	dependent continuous	Pearson correlation	< 0.0001
Results text	2 groups, 2 outcomes	Fisher's exact text	0.0135
Figure 5B (6wpc vs CNTF + 6wpc)	non-normal distribution	Mann Whitney test	0.0001
Figure 5C	normal distribution, unequal variance	Welch's test	< 0.0001
Figure 5D	normal distribution, unequal variance	Welch's test	0.1152
Figure 5E	normal distribution, unequal variance	Welch's test	< 0.0001